Progress In Electromagnetics Research B, Vol. 101, 137–154, 2023

A MIMO PIFA Loaded with CSRR-SRR Quadruplets for WLAN, ISM Band, and S-/C-Band Wireless Applications

Srujana Vahini Nandigama*, Kunooru Bharath, and Rama Krishna Dasari

Abstract—The article presents a multiband symmetrically placed two elements, inverted-F multiple inputs multiple outputs (MIMO) antenna for wireless LAN (WLAN), Industrial, Society and Medical (ISM) band, S-/C-band applications. Decoupling ($S_{12} < -15$ dB) between the two antenna elements of MIMO antenna is improved by introducing metallic vias at the top ends of the patch. The MIMO antenna has been fabricated and measured on a piece of low-cost, low-profile, FR-4 substrate. A combination of parasitic loading of 4-units (quadruplet) of square-split ring resonators (SRRs) and complementary split ring resonator (CSRR) cells have been used to achieve quad-bands for lower than -10 dB total active reflection coefficients and additionally to improve the isolation between antenna elements. The paper also presents the tabularized and graphical investigations of the analyzed and measured resultant MIMO parameters like envelope correlation coefficient (ECC), diversity gain (DG), total active reflection coefficients (TARC), MIMO-VSWR (voltage standing wave ratio), channel capacity loss (CCL), etc. and are found approximately close to each other with small acceptable errors. The other important parameters (reflection coefficients, radiation pattern, E-plane and H-plane polar plots, electric field vector (E) distribution, and current density vector (J) distribution) of the proposed antenna were also demonstrated and measured using a vector network analyzer (Agilent N5247A VNA) and 18 GHz anechoic chamber in the microwave research laboratory. The MIMO (1×2) antenna is best suitable for Bluetooth/WLAN/Wi-Fi (2.45–2.57 GHz) and ISM band, FIXED, MOBILE, RADIO Location, Amateur & Amateur-satellite service (2.45 GHz) within impedance bandwidth ($S_{11} < -10$ dB) from 2.45–2.57 GHz lower band, midband at 4.4 GHz, and n46 (5.40–5.49 GHz) upper band.

1. INTRODUCTION

Researchers and scientists have developed a single unit of the number of antennas using metamaterials SRR, CSRR, PIN diodes, varactor diodes, electromagnetic band gap (EBG) structures, defected ground structure (DGS), metasurface-based, frequency selective surface based, metamaterial absorber, superstrate structure, meandered lines, lumped elements, etc. [1–10] to make a wireless communication system more efficient and faster. Improved spectrum usage and reliable data transmission are both greatly aided by multiple-input multiple-output (MIMO) technologies. Moreover, high isolation and miniaturization are becoming essential developments for MIMO antenna systems. Yet for numerous antennas, port isolation and downsizing have always been mutually exclusive. MIMO is most popular nowadays because of its performance parameters, the suitable high-speed data rate for 5G and higher mobile technologies, and the diversity of parameters in modern microwave and millimeter-wave band applications. Deng et al. proposed a linearly polarized 2×2 MIMO antenna that exhibited dual band performance for WLAN and Wi-Fi applications. Isolation enhancement was achieved by the use of a T-slot and meander line (ML) in the bottom ground. The authors also explained the plots of ECC and the total efficiency of the MIMO antenna [11]. Li et al. proposed two methods of reducing mutual coupling

Received 5 May 2023, Accepted 8 July 2023, Scheduled 23 July 2023
* Corresponding author: Srujana Vahini Nandigama (srujana.nandigama@gmail.com).
The authors are with the Centre for Excellence in Microwave Engineering, Osmania University, Hyderabad, India.

between two antenna elements using meandered lines (MLs) and inserting a slot in the ground plane [12]. Nadeem and Choi have collected different MIMO design techniques and compared mutual coupling reduction techniques [13]. Zhao and Wu developed a coupled resonator decoupling network to reduce the coupling coefficient between the two coupled antennas for 2.4 GHz and 5.2 GHz frequency bands [14]. Mashagba et al. elaborated a mutual coupling reduction method using a slit and split ring for a dual-band MIMO antenna for a wireless body area network (WBAN) and 5G wireless applications [15]. Guo et al. collected and demonstrated different mutual coupling reduction methods. Lumped element, coupled resonators, neutralization lines, parasitic resonant units, defected ground structures, pattern diversity, mode diversity, electromagnetic band gap structures, spoof surface plasmon polariton, frequency selected surface, metasurface based decoupling methods are mainly employed for MIMO antennas [16]. Al-Hasan et al. demonstrated an mm-wave MIMO antenna with mutual coupling reduction using a hybrid isolator [17]. Lee and Jang presented a 2×2 MIMO antenna using two non-similar antenna elements and achieved enhanced isolation by reduced correlation instead of using identical types of antennas. MIMO antenna comprises a PIFA and a coupling antenna with the property of a loop [18]. Iqbal et al. developed a compact UWB-MIMO antenna with a reduced isolation coefficient ($S_{12} < -20\,\text{dB}$) using two monopoles and defective ground using two inverted F stubs [19]. Zhang et al. used the metamaterial absorber to reduce mutual coupling between the two identical impedance transformers fed MIMO elements [20]. Alibakhshikenari et al. demonstrated a method of mutual coupling suppression for a planar phased array using a metamaterial superstrate between two radiating elements [21].

The primary objective of the proposed scheme is to achieve multi-narrow band 1×2 MIMO antennas and improve the isolation between them using shorting metallic vias and parasitic loading of quadruplet SRR units for WLAN, ISM band, and S-band and C-band wireless applications. Another objective of this research is to improve the MIMO diversity parameters TARC, VSWR-MIMO, ECC, DG, and CCL and validation of these diversity parameters by the measured S-parameters of the fabricated antenna prototype model.

This work discusses the fabrication analysis and investigation of the two elements two port inverted-F MIMO antenna using quadruplet parasitic loading of SRR and CSRR. The proposed antenna is an extension of the research work done by Deng et al., 2017 [11]. In this proposed work, MIMO parameters of the antenna have been analysed and measured. The MIMO diversity parameters have been evaluated using HFSS software and measured and verified in the succeeding section using Vector Network Analyser (Agilent N5247A VNA), and radiation patterns and gain are observed in an 18 GHz anechoic chamber.

2. MATERIALS AND METHODS

The proposed antenna is designed at a frequency of 2.52 GHz. The designed symmetrically placed two elements 1×2 MIMO antenna is fabricated on a low-profile FR-4 substrate ($\varepsilon_r = 4.4$, $\tan\delta = 0.02$) of pieces 52 mm wide and 77.5 mm long. The height of the chosen substrate is 1.6 mm.

2.1. Antenna Geometry

The basic PIFA element is designed for dual bands and the lengths of both arms corresponding to wavelengths of each frequency, i.e., 2.52 GHz and 5.4 GHz. The inclusion of metamaterial unit cells as a parasitic element on the top layer added two more frequency bands around 3.9 GHz and 4.7 GHz because the SRR unit cell loops lengths are related to the corresponding frequencies. Two metallic shorting vias of radius 0.5 mm, along with the quadruplets of square split ring resonators (S-SRRs) {outer square side length = 4.0 mm, inner square side length = 3 mm, gap between two rings = 0.2 mm, each square ring thickness = 0.3 mm, and cut inside arms = 0.6 mm} have been used for the improvement of isolation coefficient or decoupling between the two antenna elements. The first S-SRR unit is placed in the middle of the substrate width between the two patches at a height of 1.75 mm, and the next S-SRR rings are placed with a gap of 0.5 mm along length. The spatial distance between the two antennas is 21.60 mm. All the corners of the patch are filleted with a 1.0 mm distance to overcome the effect of electrons cloud at the corners. The two 2.5 mm wide inverted-F patches are placed at a distance of 12 mm from the bottom end as illustrated in the left-hand side of Fig. 1(a). Two 0.16 mm thick C-slots are introduced in the patch to achieve impedance matching as shown in Fig. 1(b). The bottom of the

antenna comprises a ground (52 mm × 70 mm), T-slot, and quadruplets of square complementary split ring resonator (S-CSRR). Each unit cell of S-CSRR has the same dimensions as that of a unit cell of S-SRR. A combination of S-CSRRs (four) is placed at a distance of 18.75 mm from the bottom end of the ground. A T-slot is placed at a distance of 2.5 mm from the bottom end of the ground; the base of the T-arm is 29.85 mm along with a width of 2 mm; and the T-arm cut width is 1.6 mm as displayed on the right-hand side of Fig. 1(a). Nine 0.2 mm × 70 mm meandered line (ML) sections are attached to the ground in the middle of the T-slot as represented in Fig. 1(c) and Fig. 1(d).

2.2. Effect of MIMO Parasitic Loading with SRR Units

The effect of the increased number of parasitic square-SRR (S-SRR) unit cells has been tabularized in Table 1. The table is divided into two sections. In the first section, the left-hand side (LHS) shows

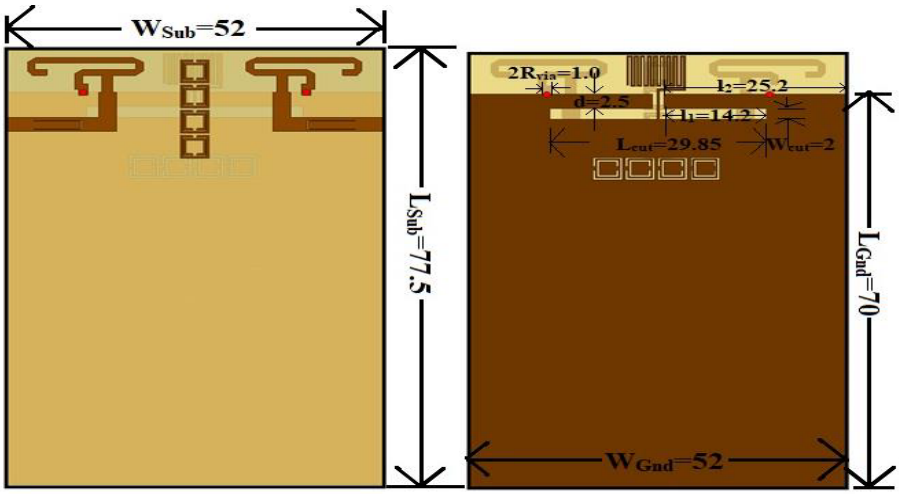

(a)

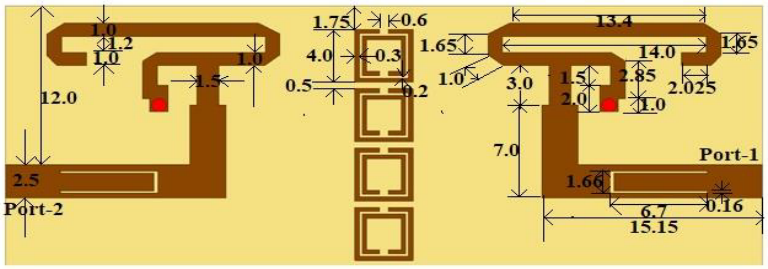

(b)

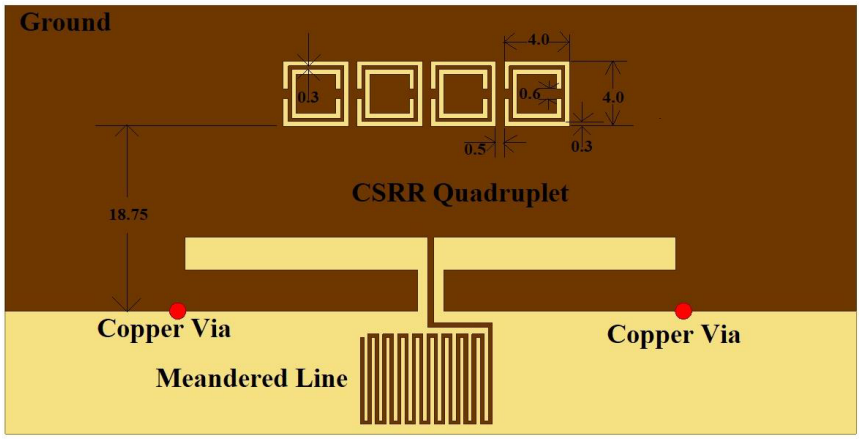

(c)

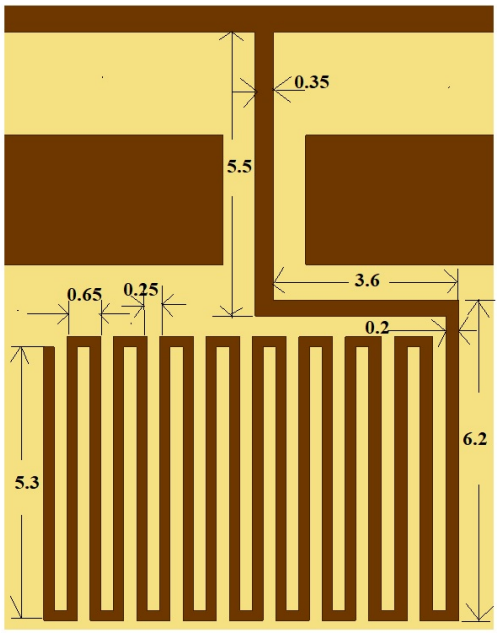

(d)

Figure 1. MIMO antenna configuration and its dimensional (in mm) representation.

Table 1. Effect of MIMO parasitic loading with SRR units.

No. of S-SRR	N	f_r (GHz)	Bands (f_L-f_H GHz)	FBW (%)	S_{11} (dB)	S_{12} (dB)	MIMO Diversity Parameters				
							TARC (dB)	VSWR	ECC	DG (dB)	CCL (bit/s/Hz)
Without SRR	4	2.52	2.47–2.57	3.96	−21.2	−19.87	−5.66	1.35	0.02	9.998	1.61
		3.68	3.65–3.69	1.087	−10.67	−24.16	−4.58	1.57	0.002	9.999	1.30
		4.12	4.06–4.18	2.91	−16.13	−9.85	−21.94	1.16	0.04	9.992	0.64
		4.83	4.82–4.84	0.414	−10.24	−15.62	−7.32	1.03	0.002	9.999	0.55
1-SRR	3	2.52	2.46–2.58	4.76	−30.89	−14.79	−9.12	1.29	0.02	9.998	0.74
		4.04	3.99–4.11	2.97	−16.09	−11.86	−15.92	1.08	0.03	9.995	0.56
		4.72	4.66–4.77	2.33	−12.76	−13.78	−6.02	1.25	0.01	9.999	0.58
2-SRR	4	2.50	2.45–2.57	4.80	−23.80	−15.13	−8.62	1.13	0.02	9.998	0.85
		3.97	3.94–3.99	1.25	−10.60	−10.89	−17.0	1.07	0.05	9.989	0.67
		4.44	4.43–4.45	0.45	−10.43	−12.80	−2.97	5.96	0.09	9.956	1.25
		4.72	4.66–4.77	2.33	−12.79	−13.67	−6.93	1.21	0.004	9.999	0.57
3-SRR	3	2.50	2.45–2.57	4.80	−21.80	−14.73	−9.37	1.03	0.02	9.998	0.78
		4.67	4.61–4.72	2.35	−13.54	−15.04	−7.53	1.26	0.004	9.999	0.52
		5.40	5.37–5.43	1.11	−10.96	−18.58	−16.48	1.34	0.01	9.999	0.34
4-SRR	4	2.52	2.45–2.57	4.76	−20.36	−15.17	−10.44	1.86	0.02	9.999	0.72
		3.94	3.91–3.96	1.27	−10.70	−10.97	−16.13	1.37	0.06	9.98	0.71
		4.70	4.64–4.77	2.76	−14.12	−14.08	−11.09	1.77	0.01	9.999	0.62
		5.44	5.40–5.49	1.65	−11.78	−20.53	−10.81	1.80	0.002	9.998	0.30

***N=Number of Bands; f_r=Resonance Frequency; S_{11}=Reflection coefficient; S_{12}=Isolation coefficient**

the resonant frequencies, number of bands, −10 dB fractional bandwidth (FBW), reflection coefficients (S_{11}), and isolation coefficients (S_{12}). On the other hand, the right-hand side (RHS) section comprises the MIMO diversity parameters like TARC, VSWR, ECC, DG, and CCL. It has been observed from the compared data that when the MIMO system is unloaded with S-SRR units the isolation coefficient is above −10 dB as parasitic loading with the number of S-SRR unit cells increases the isolation, or the decoupling between the two antenna patch elements downs its value below −10 dB. The lowest decoupling values for all four resonating narrow bands are achieved with parasitic loading of quadruplets of S-SRRs over the full band from 2 GHz to 6 GHz. The reflection and isolation coefficients family of curves of each S-SRR parasitic loading effect are illustrated in Fig. 2(a) and Fig. 2(b), respectively. All diversity parameters come within the threshold limits.

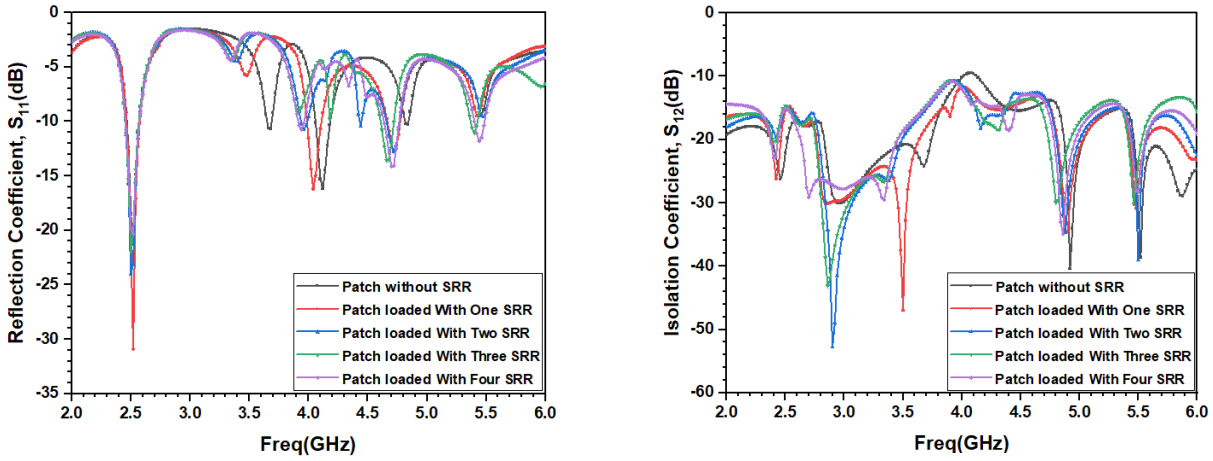

Figure 2. Effect of MIMO antenna parasitic loading with SRR units. (a) Reflection coefficient, S_{11}. (b) Isolation coefficient, S_{12}.

2.3. Effect of Introduced C-slot in the Patch

A C-slot is introduced in the patch, and the effect of introduced slots in the MIMO antenna system is shown in Table 2 concerning the MIMO antenna system without slots. The reflection coefficients and isolation coefficients without and with introduced C-slots are compared in Fig. 3(a) and Fig. 3(b), respectively. It is observed from the table data that the total active reflection coefficient is improved for all four resonating bands below −10 dB. The MIMO diversity gain is close to 10 dB, and channel capacity loss is also improved.

Table 2. Effect of introduced C-slots in the patch.

Patch with C-Slots	N	f_r (GHz)	Bands (f_L-f_H GHz)	FBW (%)	S_{11} (dB)	S_{12} (dB)	MIMO Diversity Parameters				
							TARC (dB)	VSWR	ECC	DG (dB)	CCL (bit/s/Hz)
Without C-Slots	3	2.52	2.46–2.58	4.76	−22.24	−14.29	−9.89	1.01	0.03	9.996	0.83
		4.62	4.56–4.67	2.38	−13.29	−15.43	−6.74	1.79	0.005	9.999	0.63
		5.30	5.28–5.33	0.94	−10.50	−16.58	−15.92	1.36	0.01	9.999	0.42
With C-Slots	4	2.52	2.45–2.57	4.76	−20.36	−15.17	−10.44	1.86	0.02	9.999	0.72
		3.94	3.91–3.96	1.27	−10.70	−10.97	−16.13	1.37	0.06	9.98	0.71
		4.70	4.64–4.77	2.76	−14.12	−14.08	−11.09	1.77	0.01	9.999	0.62
		5.44	5.40–5.49	1.65	−11.78	−20.53	−10.81	1.80	0.002	9.998	0.30

***N=Number of Bands; f_r=Resonance Frequency; S_{11}=Reflection coefficient; S_{12}=Isolation coefficient**

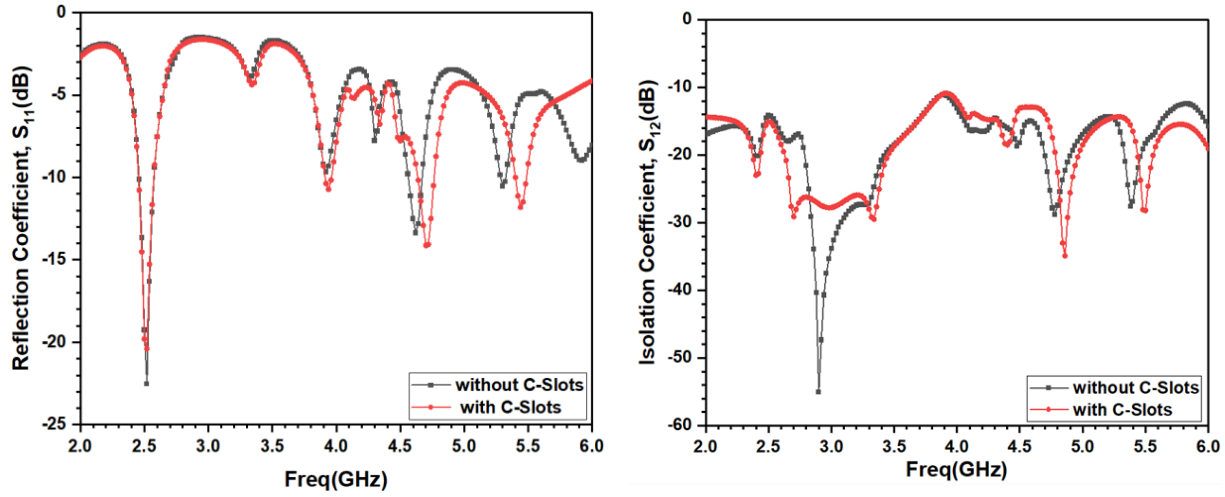

Figure 3. Effect of introduced C-slots in the patch. (a) Reflection coefficient, S_{11}. (b) Isolation coefficient, S_{12}.

Table 3. Effect of metallic via on MIMO antenna.

Adding of Via	N	f_r (GHz)	Bands (f_L-f_H GHz)	FBW (%)	S_{11} (dB)	S_{12} (dB)	MIMO Diversity Parameters				
							TARC (dB)	VSWR	ECC	DG (dB)	CCL (bit/s/Hz)
Without Via	2	3.46	3.40–3.50	2.89	−13.87	−13.09	−9.89	1.75	0.07	9.98	1.20
		4.12	4.07–4.18	2.66	−12.59	−8.22	−17.72	1.14	0.07	9.97	0.83
With 2 Via	4	2.52	2.45–2.57	4.76	−20.36	−15.17	−10.44	1.86	0.02	9.999	0.72
		3.94	3.91–3.96	1.27	−10.70	−10.97	−16.13	1.37	0.06	9.98	0.71
		4.70	4.64–4.77	2.76	−14.12	−14.08	−11.09	1.77	0.01	9.999	0.62
		5.44	5.40–5.49	1.65	−11.78	−20.53	−10.81	1.80	0.002	9.998	0.30

***N=Number of Bands; f_r=Resonance Frequency; S_{11}=Reflection coefficient; S_{12}=Isolation coefficient**

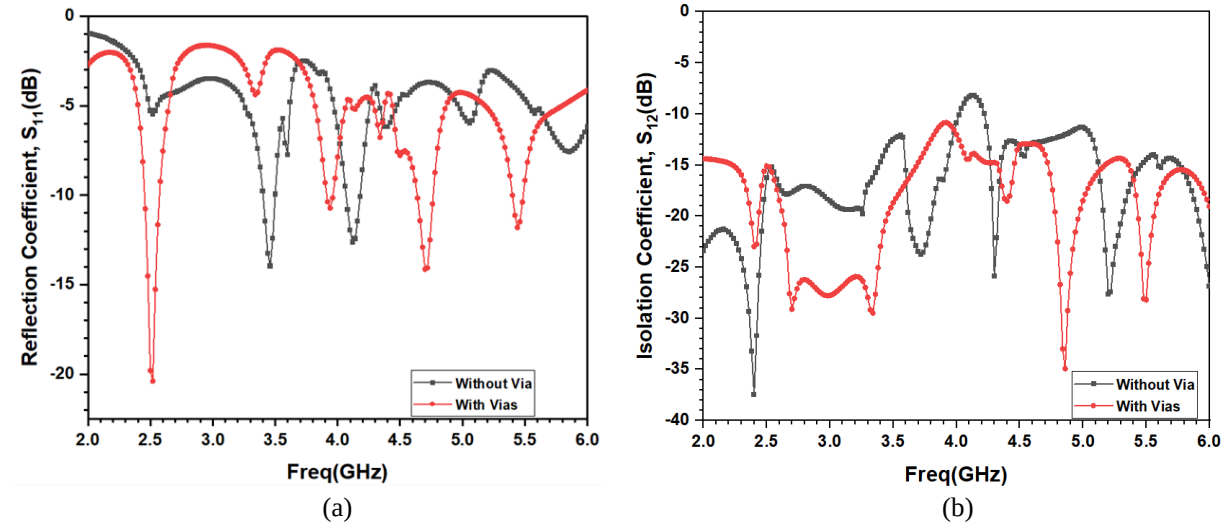

Figure 4. Effect of introduced metallic via. (a) Reflection coefficient, S_{11}. (b) Isolation coefficient, S_{12}.

2.4. Effect of Adding Metallic Via

Two metallic vias are introduced on the top edge of the two patches. The addition of via is used to short the patch with the ground. The introduced via not only downs the TARC, reflection coefficient but also tremendously reduces the isolation coefficient below −15 dB over the full band from 2 GHz to 6 GHz. The effect of the addition of via is shown in Table 3, and reflection and isolation coefficients are displayed in Fig. 4(a) and Fig. 4(b), respectively.

2.5. Effect of CSRR Quadruplet Loading on Ground

The 1 × 2 MIMO ground is loaded symmetrically with square complementary split ring resonators (S-CSRRs). The number of S-CSRR units is increased in the ground in pairs of two. The reflection coefficient and isolation coefficient plots are plotted in Fig. 5(a) and Fig. 5(b), respectively, and the comparison of resultant data of the increased number of S-CSRR units is displayed in Table 4. It is noticed from the table and family of plots that the introduced loading of S-CSRR in the ground plays a role in fine-tuning or impedance match in resonance frequency and maintaining the isolation below −15 dB.

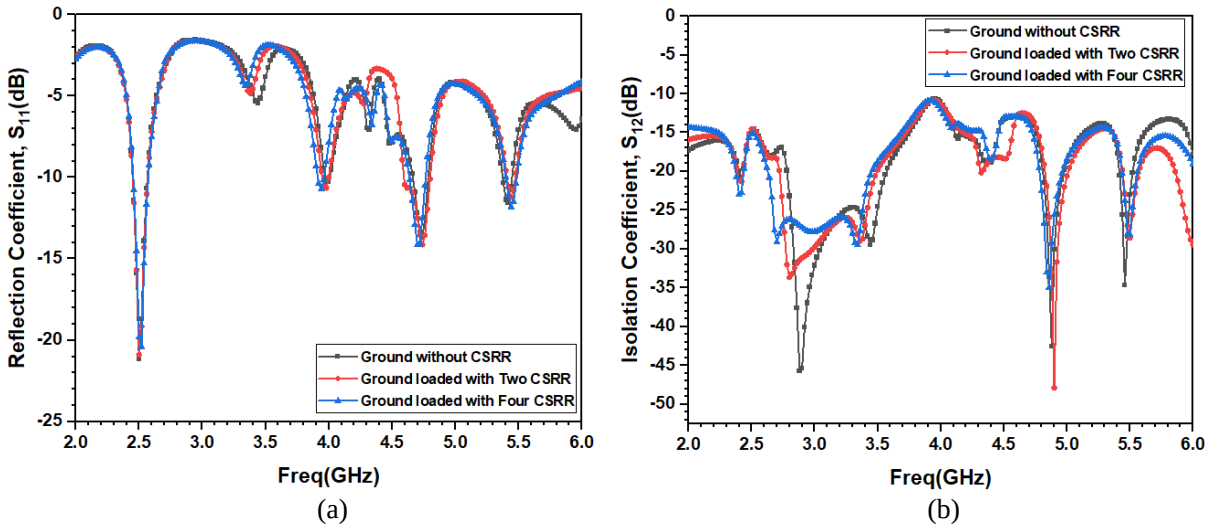

Figure 5. Effect of MIMO antenna ground parasitic loading with CSRR units. (a) Reflection coefficient, S_{11}. (b) Isolation coefficient, S_{12}.

2.6. Effect of Ground Loading with Meander Line and T-Slot

After the CSRR loading, the ground is further loaded with an additional T-slot and meander line at the bottom end as shown in Fig. 1(d). The effect of MIMO antenna ground loading with meander line and T-slot has been represented in Table 5, and their reflection coefficient and isolation coefficient are shown in Fig. 6(a) and Fig. 6(b), respectively. It has been recorded and noticed from the curves that the isolation strongly goes down below −15 dB with the insertion of the T-slot and meander line over the full band of interest. The introduced T-slot and meander line not only increase the number of resonating frequencies and hence the number of four bands below −10 dB reflection coefficient but also shrink the −10 dB fractional bandwidth from 16.60% to 1.65%.

2.7. Effect of SRR and CSRR Loading

The combined effect of introducing parasitic loading of quadruplet S-SRR unit cells on the top side and quadruplet loading of S-CSRR unit cells on the bottom side has been analysed and investigated. The comparative parameters are shown in Table 6, and their reflection and isolation family of curves are

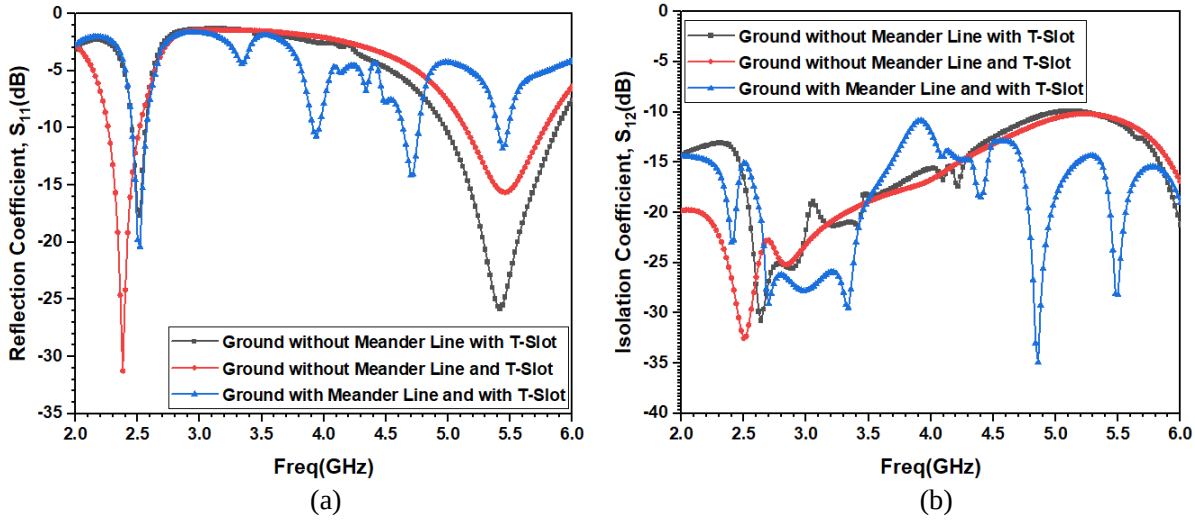

Figure 6. Effect of MIMO antenna ground loading with meander line and T-slot. (a) Reflection coefficient, S_{11}. (b) Isolation coefficient, S_{12}.

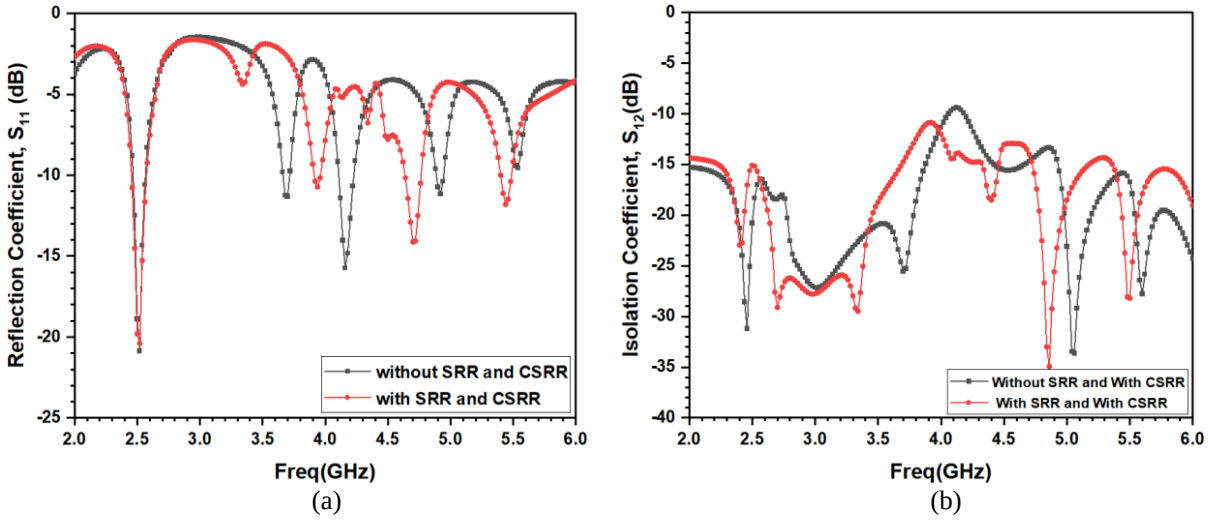

Figure 7. Effect of CSRR and SRR loading. (a) Reflection coefficient, S_{11}. (b) Isolation coefficient, S_{12}.

displayed in Fig. 7(a) and Fig. 7(b). After the loading with CSRR and SRR units, the first frequency band (2.45–2.57 GHz) does not change while the resonating frequencies and their corresponding frequency bands are either shifted towards the right or left as compared to the unloaded S-SRR or S-CSRR.

3. RESULTS AND DISCUSSIONS

3.1. 1 × 2 MIMO Model Fabrication and Measurements

The 1×2 MIMO antenna model is fabricated on the low-cost, low-profile FR-4 substrate by film-making, photolithography, and chemical etching process. The fabricated two-port model's front and rear views are shown in Fig. 8(a). Then prototype S-parameters are measured in a microwave laboratory by using Vector Network Analyzer (Agilent N5247A), and radiation patterns and gain are measured in an 18 GHz anechoic chamber as shown in Fig. 8(b).

Table 4. Effect of MIMO antenna ground loading with S-CSRR units.

No. of S-CSRR	N	f_r (GHz)	Bands (f_L-f_H GHz)	FBW (%)	S_{11} (dB)	S_{12} (dB)	MIMO Diversity Parameters				
							TARC (dB)	VSWR	ECC	DG (dB)	CCL (bit/s/Hz)
Without CSRR	4	2.50	2.45–2.57	4.80	−20.96	−14.67	−9.63	1.11	0.02	9.997	0.72
		3.99	3.97–4.01	1.00	−10.26	−10.95	−18.41	1.07	0.05	9.99	0.68
		4.74	4.66–4.79	2.74	−13.66	−14.13	−6.56	1.22	0.01	9.999	0.60
		5.41	5.37–5.45	1.48	−11.47	−19.22	−17.08	1.25	0.003	9.999	0.28
With 2 CSRR	4	2.50	2.45–2.57	4.80	−20.70	−14.55	−10.46	1.07	0.02	9.998	0.65
		3.98	3.95–4.00	1.25	−10.62	−10.99	−17.08	1.02	0.05	9.99	0.70
		4.74	4.43–4.45	0.42	−14.09	−13.59	−6.02	1.13	0.01	9.998	0.61
		5.44	5.41–5.47	1.10	−11.15	−20.00	−17.08	1.07	0.004	9.999	0.30
With 4 CSRR	4	2.52	2.45–2.57	4.76	−20.36	−15.17	−10.44	1.86	0.02	9.999	0.72
		3.94	3.91–3.96	1.26	−10.70	−10.97	−16.13	1.37	0.06	9.98	0.71
		4.70	4.64–4.77	2.76	−14.12	−14.08	−11.09	1.77	0.01	9.999	0.62
		5.44	5.40–5.49	1.65	−11.78	−20.53	−10.81	1.80	0.002	9.998	0.30

***N=Number of Bands; f_r=Resonance Frequency; S_{11}=Reflection coefficient; S_{12}=Isolation coefficient**

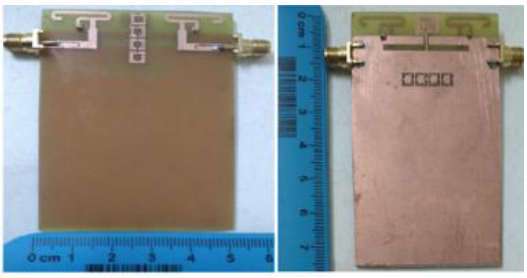

(a)

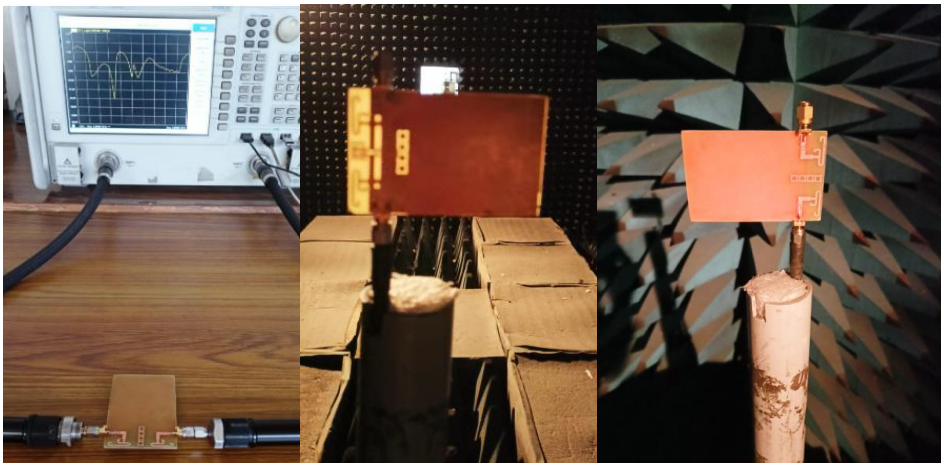

(b)

Figure 8. 1×2 MIMO antenna. (a) Fabricated prototype. (b) Laboratory measurements.

Table 5. Effect of MIMO antenna ground loading with meander line and T-slot.

Loading With ML	N	f_r (GHz)	Bands (f_L-f_H GHz)	FBW (%)	S_{11} (dB)	S_{12} (dB)	MIMO Diversity Parameters				
							TARC (dB)	VSWR	ECC	DG (dB)	CCL (bit/s/Hz)
Without ML and with T-slot	2	2.52	2.46–2.56	3.97	−17.66	−17.78	−5.51	1.02	0.06	9.98	2.47
		5.42	4.98–5.88	16.6	−25.74	−10.66	−13.55	1.05	0.004	9.999	0.29
No ML and T-Slot	2	2.38	2.26–2.52	1.09	−31.23	−25.43	−4.43	2.20	0.01	9.999	2.33
		5.46	5.14–5.78	1.17	−15.63	−10.60	−19.17	1.11	0.02	9.998	0.39
With ML and T-Slot	4	2.52	2.45–2.57	4.76	−20.36	−15.17	−10.44	1.86	0.02	9.999	0.72
		3.94	3.91–3.96	1.26	−10.70	−10.97	−16.13	1.37	0.06	9.98	0.71
		4.70	4.64–4.77	2.76	−14.12	−14.08	−11.09	1.77	0.01	9.999	0.62
		5.44	5.40–5.49	1.65	−11.78	−20.53	−10.81	1.80	0.002	9.998	0.30

***ML=Meander line; *N=Number of Bands; f_r=Resonance Frequency; S_{11}=Reflection coefficient; S_{12}=Isolation coefficient**

Table 6. Effect of CSRR and SRR loading.

SRR and CSRR	N	f_r (GHz)	Bands (f_L-f_H GHz)	FBW (%)	S_{11} (dB)	S_{12} (dB)	MIMO Diversity Parameters				
							TARC (dB)	VSWR	ECC	DG (dB)	CCL (bit/s/Hz)
No SRR and CSRR	4	2.52	2.47–2.57	3.96	−20.70	−18.60	−6.02	1.73	0.01	9.999	0.89
		3.70	3.66–3.72	1.62	−11.30	−25.55	−4.73	1.73	0.002	10.0	1.61
		4.16	4.18–4.23	1.20	−15.60	−9.67	−20.0	1.21	0.04	9.991	0.65
		4.92	4.89–4.95	1.22	−11.15	−14.44	−8.18	1.19	0.037	10.0	0.45
With SRR and CSRR	4	2.52	2.42–2.57	4.76	−20.36	−15.17	−10.44	1.86	0.02	9.999	0.72
		3.94	3.91–3.96	1.27	−10.70	−10.97	−16.13	1.37	0.06	9.98	0.71
		4.70	4.64–4.77	2.76	−14.12	−14.08	−11.09	1.77	0.01	9.999	0.62
		5.44	5.40–5.49	1.65	−11.78	−20.53	−10.81	1.80	0.002	9.998	0.30

***N=Number of Bands; f_r=Resonance Frequency; S_{11}=Reflection coefficient; S_{12}=Isolation coefficient**

3.2. Reflection and Isolation Coefficients

The measured and simulated reflection coefficients (S_{11}/S_{22}) and decoupling or isolation coefficients (S_{12}/S_{21}) are graphically compared in Fig. 9(a) and Fig. 9(b). The measured reflection coefficient plot is found near the simulated reflection coefficient curve. On the other hand, the measured isolation coefficient plot is better than the simulated one with isolation lower than −15 dB over the full frequency range from 2.0 GHz to 6.0 GHz. The simulated and measured S-parameter results are compared in Table 7.

3.3. Radiation Patterns

The simulated radiation E-plane and H-plane patterns and 18 GHz anechoic chamber measured E-plane and H-plane radiation patterns are plotted on the same polar plot at frequencies 2.52 GHz, 4.40 GHz, and 5.50 GHz and represented in Figs. 10(a)–(c), respectively. The three-dimensional gain radiation patterns at frequencies 2.52 GHz, 4.40 GHz, and 5.50 GHz are shown in Figs. 11(a)–(c). The radiation pattern at a frequency of 2.52 GHz is shown on the MIMO antenna in Fig. 11(d). In an E-plane, the radiation pattern is bidirectional while in an H-plane pattern radiation is more in the front direction than the back lobe. This implies a higher front-to-back lobe ratio (FBR), i.e., 17.5 dB. The measured and simulated radiation patterns are found approximately similar to each other at frequencies 2.52 GHz, 4.40 GHz,

Table 7. Simulated vs measured S-parameters results.

Results	N	f_r (GHz)	Bands (f_L-f_H GHz)	FBW (%)	S_{11} (dB)	S_{12} (dB)
Simulated	4	2.52	2.45–2.57	4.76	−20.36	−15.17
		3.94	3.91–3.96	1.27	−10.70	−10.97
		4.70	4.64–4.77	2.76	−14.12	−14.08
		5.44	5.40–5.49	1.65	−11.78	−20.53
Measured	4	2.53	2.42–2.72	11.85	−31.32	−21.80
		4.0	3.95–4.06	2.75	−13.19	−16.55
		4.53	4.40–4.93	11.69	−13.97	−18.87
		5.47	5.41–5.51	1.83	−13.19	−27.86

***N=Number of Bands; f_r=Resonance Frequency; S_{11}=Reflection coefficient; S_{12}=Isolation coefficient**

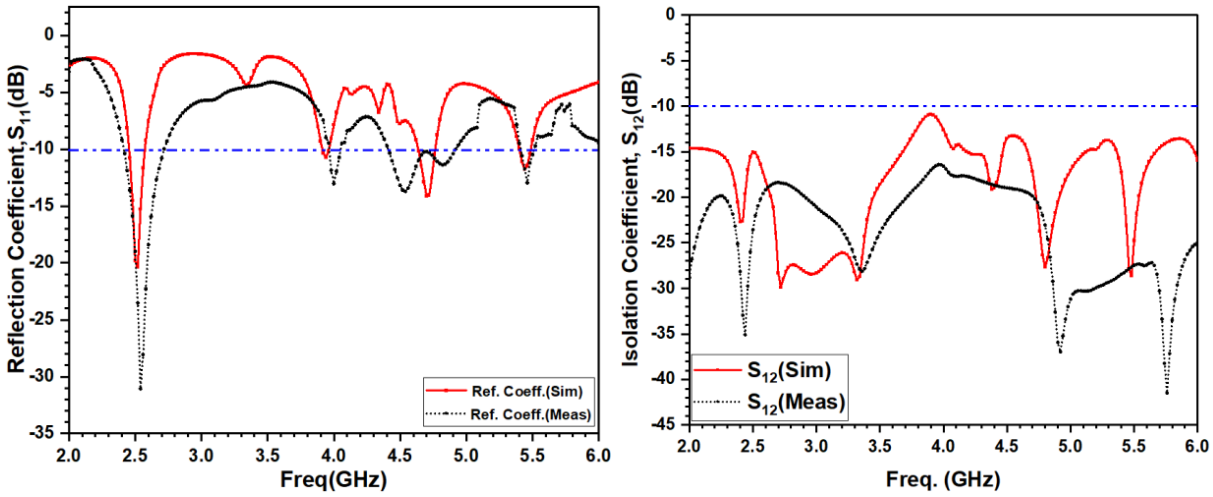

(a) (b)

Figure 9. The proposed MIMO antenna S-parameters (sim vs meas). (a) Reflection coefficient, S_{11}. (b) Isolation coefficient, S_{12}.

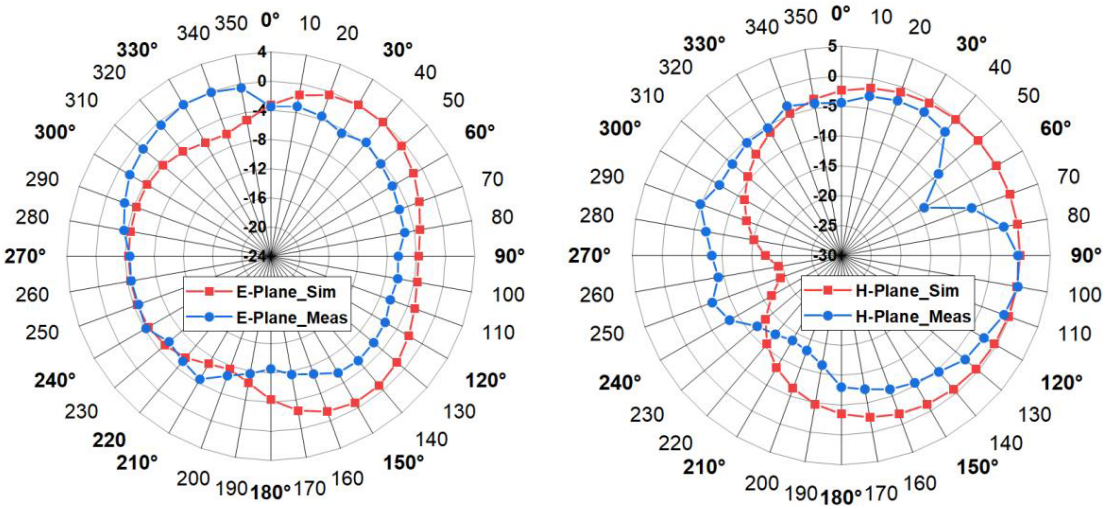

(a)

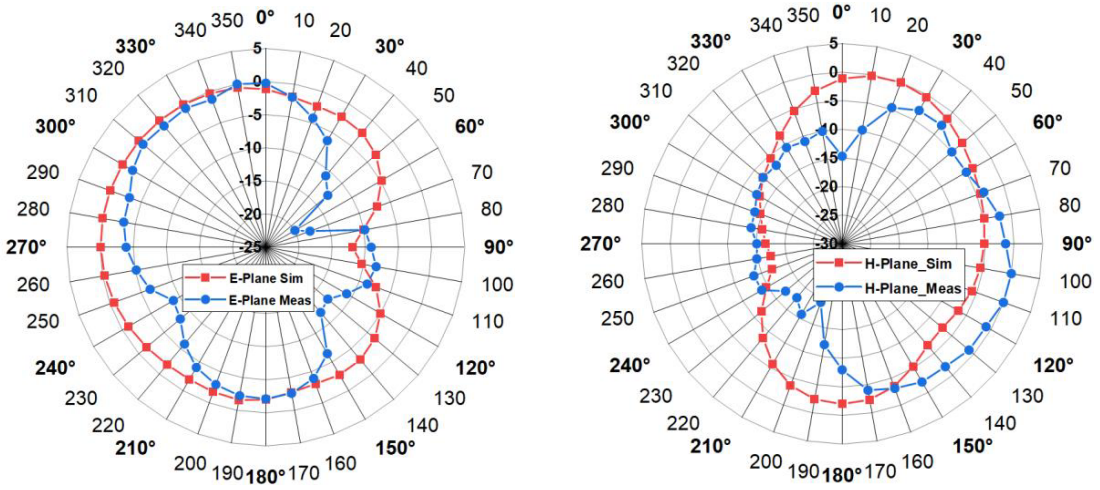

(b)

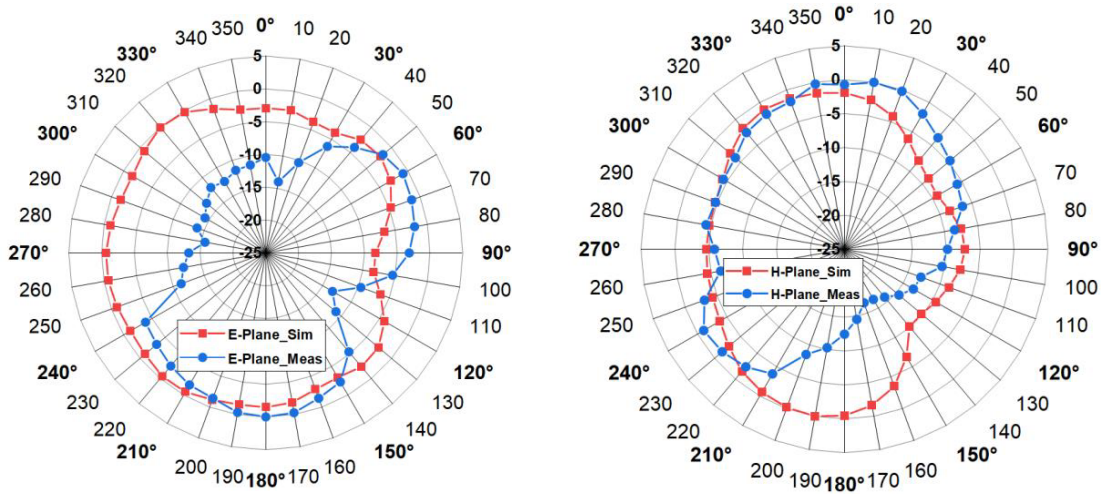

(c)

Figure 10. Normalized E-plane and H-plane patterns with Phi $= 0°$ and Phi $= 90°$, (a) at 2.52 GHz, (b) at 4.4 GHz, (c) at 5.50 GHz.

and 5.50 GHz. The maximum realized gain simulated values at frequencies 2.52 GHz, 4.40 GHz, and 5.50 GHz are 3.93 dBi, 5.42 dBi, and 5.17 dBi, respectively.

3.4. MIMO Diversity Parameters

The main diversity parameters like total active reflection coefficient (TARC), VSWR-MIMO, envelope correlation coefficient (ECC), Diversity gain (DG), and channel capacity loss (CCL) from the simulated and measured S-parameters for 1×2 MIMO antenna have been evaluated and compared in Figs. 12(a)–(d). Both measured and software-simulated results are found in closed matching and within the specified threshold limits [15, 19, 22–24]. The dotted lines in the comparison plots are representing the measured curves while the solid lines indicate the simulated results. The TARC is below -10 dB for all four resonating bands with an acceptable shift in the frequency bands as illustrated in Fig. 12(a). The VSWR-MIMO is below 2.0 for all four resonating bands with an acceptable shift in the frequency bands as illustrated in Fig. 12(b). This ensures that the antenna is suitable for diverse applications. The ECC and diversity gain are in great concord with simulated ECC and DG values as displayed in Fig. 12(c). The measured ECC values are lower than 0.1, and DG values are close to 10 for all four obtained

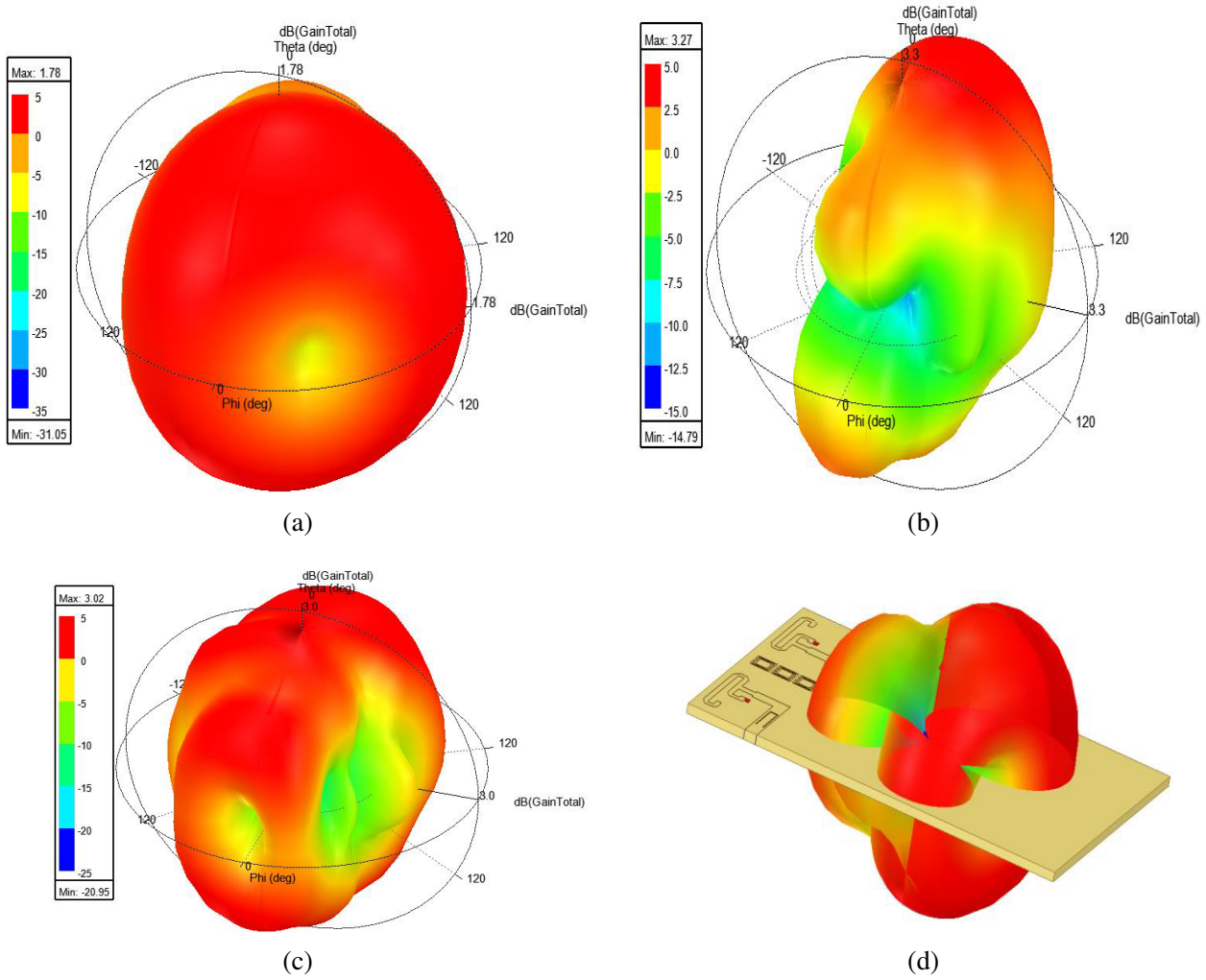

Figure 11. 3-D E-plane and H-plane radiation patterns with Phi = 0° and Phi = 90°, (a) at 2.52 GHz, (b) at 4.4 GHz, (c) at 5.5 GHz, (d) radiation pattern on MIMO antenna.

Table 8. Simulated vs measured MIMO diversity-parameters results.

Results	***N***	***f_r*** **(GHz)**	**TARC (dB)**	**VSWR (MIMO)**	**ECC**	**DG (dB)**	**CCL (bit/sec/Hz)**
Simulated	4	2.38	−22.81	1.156	0.03	9.999	1.92
		3.92	-22.28	1.166	0.057	9.98	0.642
		4.74	−16.10	1.371	0.016	9.999	0.468
		5.44	−17.89	1.292	0.0129	9.998	0.296
Measured	4	2.53	−20.68	1.34	0.002	9.999	0.03
		4.0	−19.33	1.76	0.02	9.999	0.21
		4.53	−16.53	1.56	0.011	9.999	0.16
		5.47	−12.53	1.61	0.011	9.999	0.23

***N=Number of Bands; f_r=Resonance Frequency**

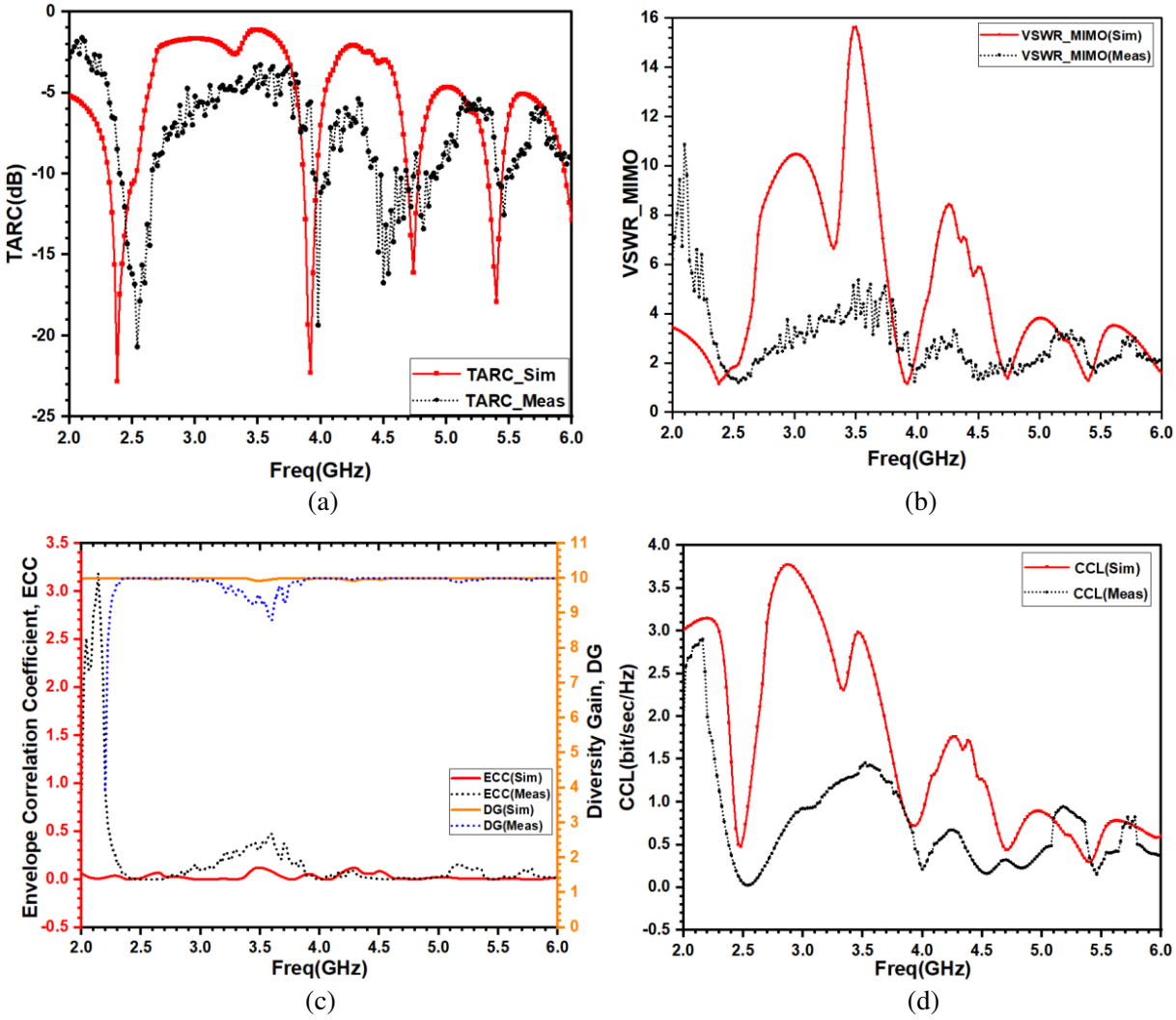

Figure 12. MIMO diversity parameters. (a) Total Active Reflection Coefficients (TARC). (b) VSWR_MIMO. (c) Envelope Correlation Coefficient (ECC) and Diversity Gain (DG). (d) Channel Capacity Loss (CCL).

−10 dB frequency bands. This ensures that the designed and developed MIMO system is excellent and has better isolation properties. The simulated and measured CCLs are compared in Fig. 12(d). The measured value of CCL is far better than the simulated CCL. It is also noticed that the measured CCL is well below 0.4 bit/sec/Hz for the four specified bands. All the measured and simulated diversity parameters are compared in Table 8.

3.5. Electric Field and Surface Current Density Vector Distribution

The electric field vector distribution is shown in Fig. 13(a). Electric field distribution in Fig. 13(a) clearly shows the radiating capability of the antenna. Both the PIFA antenna and SRR unit cells contribute to the radiation.

The surface current density vector distribution on the patch and the ground is illustrated in Fig. 13(b). Surface current density shows that meander lines, T-slot, and CSRR stop the current to flow from one antenna to another so that mutual coupling will be reduced.

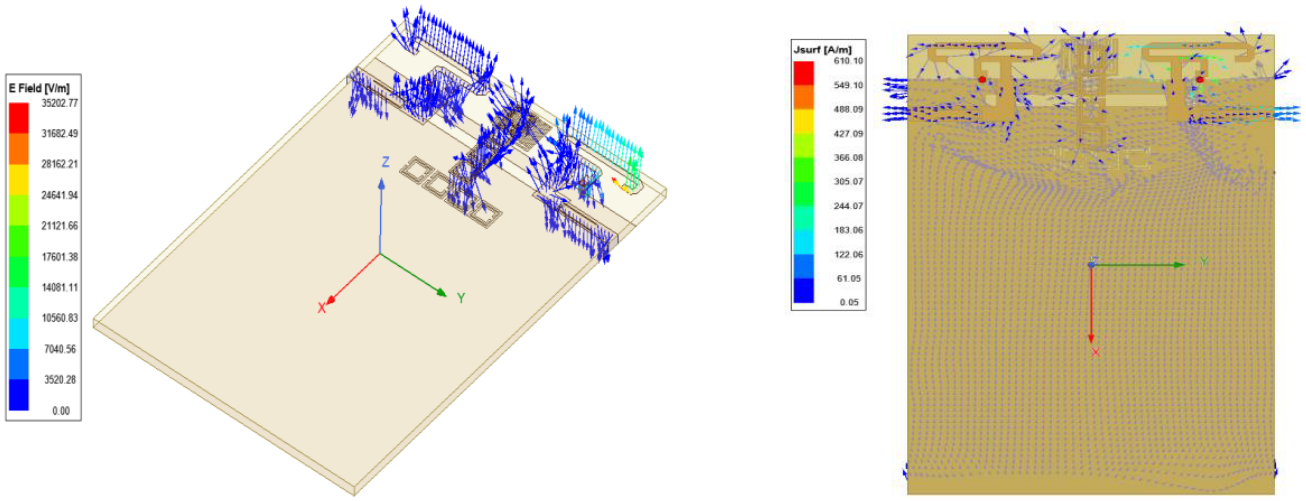

(a) (b)

Figure 13. Electric field vector distribution. (a) Electric field vector distribution. (b) Current density distribution vector at top view and bottom view.

3.6. Comparison with Previously Published Similar Works

The proposed 1×2 MIMO antenna is compared to existing similar 1×2 MIMO antennas in the literature, as shown in Table 9. Compared to other MIMO antennas, the proposed MIMO antenna offers better isolation between the ports with less complexity in the antenna structures [11, 12, 15, 18, 19]. Some

Table 9. Comparison with previously published similar works.

Ref. Year	Ant. Size (mm^2)	Sub	f_0	N	f_r	−10 dB Bands (GHz)	MIMO Diversity Parameters					
							S_{12} (dB)	TARC (dB)	VSWR	ECC	DG (dB)	CCL (bit/s/Hz)
[11] 2017	52 × 77.5	FR-4	2.4	2	2.4 5.0	2.4–2.48 5.15–5.82	< −15 < −15	NA	NA	0.04 0.20	9.991_E 9.798_E	Good (NA)
[12] 2018	60 × 78	FR-4	5.0	1	5.0	4.60–5.10	< −20	NA	NA	NA	NA	NA
[15] 2021	31 × 47.2	Felt $\varepsilon_r = 1.44$ $\tan\delta = 0.044$ $h = 3$ mm	3.5		2.45 3.5	2.39–2.50 3.38–3.62	< −30	NA	NA	< 0.05 < 0.05	≈ 10 ≈ 10	< 0.4 < 0.4
[18] 2015	60 × 115	FR-4	2.45	1	1.90	1.17–2.17 (< −6 dB)	< −20	NA	NA	< 0.02	≈ 10	NA
[19] 2018	50 × 30	FR-4	4.6	1	4.6 6.8	2.5–14.5	< −20	NA	NA	< 0.04	> 7.4	NA
This Work	52 × 77.5	FR-4	2.45	4	2.52 3.94 4.70 5.44	2.45–2.57 3.91–3.96 4.64–4.77 5.40–5.49	−15.17 −10.97 −14.08 −20.53	−10.44 −16.13 -11.09 −10.81	1.86 1.37 1.77 1.80	0.02 0.06 0.01 0.002	9.999 9.98 9.999 9.998	0.72 0.71 0.62 0.30

***NA=Not Available; N=Number of Bands; f_0=Design Frequency (GHz); f_r=Resonance Frequency (GHz); S_{12}=Isolation coefficient; E=Evaluated**

antennas use complex structures to achieve greater isolation than the proposed design. Furthermore, in comparison to previous works, in the proposed MIMO antenna, more numbers of diversity parameters are investigated, analyzed, and validated. These antenna performance parameters ensure that the proposed design is better than existing similar MIMO antennas. The proposed antenna configuration consumes less space than the antennas in [12, 15, 18, 19] which makes the antenna more suitable for modern communications.

4. CONCLUSION

The proposed 1×2 MIMO antenna has excellent isolation ($< -20\,\text{dB}$) and reflection coefficient values well below $-10\,\text{dB}$ over the ISM band (2.42–2.72 GHz), narrow band bandwidth, channel capacity loss (CCL $< 0.21\,\text{bit/sec/Hz}$), envelope correlation coefficients (ECC < 0.023), cross-correlation coefficient ($0 < \sqrt{\text{ECC}} < 0.151$), diversity gain ($9.994\,\text{dB} < \text{DG} < 9.999\,\text{dB}$), and total active reflection coefficient (TARC $= -20.68\,\text{dB}$ at 2.52 GHz), corresponding VSWR-MIMO < 2 (2.42–2.72 GHz), respectively, by the use of quadruplets Square-SRR in the patch between the two patches and square CSRR, meander line, T-slots. The two radiating patches occupy very small area on the FR4 substrate. The minimum spatial distance between the two radiating patches is less than half wavelength. Thus, each 1×2 MIMO antenna element is simple and very compact. This may result in the possibility to connect extra passive components on the surface of the patch. The radiation pattern of the antenna is bidirectional with peak gain values 3.93 dBi, 5.42 dBi, and 5.17 dBi at frequencies of 2.52 GHz, 4.40 GHz, and 5.50 GHz, respectively, and high radiation efficiency of 92.82%. The diversity performance parameter ECC is lower than 0.023, and DG ($> 9.995\,\text{dB}$) is close to 10 dB, which ensures the reliability of the signal to reach the transmitter with a high data rate. A CCL lower than $0.4\,\text{bit/sec/Hz}$ ensures an excellent signal-to-noise ratio (SNR) with the lowest interference at the far receiver end. In the future, because of the simplicity of the patch, the antenna can be used as 2×2 MIMO, 4×4 MIMO, or higher element massive MIMO systems. Four multi-band resonant frequencies are shifted in measured reflection coefficient with acceptable error shift in frequency. This is because of the soldering of the port, measuring spectrum analyzer error, and fabrication issues. After all, the measured and simulated performances of the MIMO antenna come in close agreement. Further assessments of this antenna in terms of MIMO parameters such as ECC, DG, CCL, and TARC also validate that this antenna can be potentially applied in the next generation of 5G/6G devices and can be frequency and pattern reconfigured by the use of BAR 64 02V PIN diodes. The antenna can also be used as a UWB-sensing antenna by additional attachment of varactor diodes.

ACKNOWLEDGMENT

The authors would like to convey their thanksto CEME Laboratory (ECE Dept.) at Osmania University, Hyderabad, India for providing support in the antenna design and development and also thanks to Atul Varshney (ECE Department), Gurukula Kangri (deemed to be University), Haridwar, Uttarakhand, India for providing radiation pattern measurement support.

REFERENCES

1. Varshney, A., N. Cholake, and V. Sharma, "Low-cost ELC-UWB fan-shaped antenna using parasitic SRR triplet for ISM band and PCS applications," *International Journal of Electronics Letters*, Vol. 10, No. 4, 391–402, 2022.
2. Varshney, A., et al., "Dodecagon-shaped frequency reconfigurable antenna practically loaded with 3-delta structures for ISM band and wireless applications," *IETE Journal of Research*, 1–13, Feb. 17, 2022.
3. Hussain, R. and M. S. Sharawi, "A low profile compact reconfigurable MIMO antenna for cognitive radio applications," *9th European Conference on Antennas and Propagation (EuCAP)*, 1–4, Lisbon, Portugal, 2015.

4. Shindhja, N. M. M. and Varshney, A., "Hybrid β-indexing fractal slotted multiband antenna for electronics wireless sensor applications," *Journal of Electronics, Electromedical Engineering, and Medical Informatics*, Vol. 5, No. 2, 59–68, Apr. 2023.
5. Evangelin, P. S., T. M. Neebha, A. D. Andrushia, J. Roopa Jeyasingh, A. Varshney, and X. Anitha Mary, "Design and analysis of meander slitted monopole antenna for wireless application," *2022 6th International Conference on Devices, Circuits, and Systems (ICDCS)*, 480–483, Coimbatore, India, 2022.
6. Varshney, A., V. Sharma, T. M. Neebha, and R. Kumar, "A compact low-cost impedance transformer-fed wideband monopole antenna for Wi-MAX N78-band and wireless applications," *Printed Antennas*, Vol. 1, 315–328, CRC Press, 2022.
7. Hadj Sadok, M., Y. Lamhene, and S. Berkani, "High-gain low-profile EBG resonator antenna based on quasi-icosahedral shapes," *J. Electron. Mater.*, Vol. 52, 140–152, 2023.
8. Tahseen, H. U., L. Yang, and X. Zhou, "Design of FSS-antenna-radome system for airborneand ground applications," *IET Commun.*, Vol. 15, 1691–1699, 2021.
9. Hannan, S., M. T. Islam, M. S. Soliman, M. R. Faruque, N. Misran, and M. S. Islam, "A co-polarization-insensitive metamaterial absorber for 5G n78 mobile devices at 3.5 GHz to reduce the specific absorption rate," *Scientific Reports*, Vol. 12, No. 1, 1–13, 2022.
10. Torabi, Y. and R. Omidi, "Novel metamaterial compact planar MIMO antenna systems with improved isolation for WLAN application," *Wireless Pers. Commun.*, Vol. 102, 399–410, 2018.
11. Deng, J. Y., J. Y. Li, L. Zhao, and L. X. Guo, "A dual-band inverted-F MIMO antenna with enhanced isolation for WLAN applications," *IEEE Antennas and Wireless Propagation Letters*, Vol. 16, 2270–2273, 2017.
12. Li, Q., C. Ding, R. Yang, M. Tan, G. Wu, et al., "Mutual coupling reduction between patch antennas usingmeander line," *International Journal of Antennas and Propagation*, Vol. 2018, 1–7, Article ID 2586382, Hindawi, 2018.
13. Nadeem, I. and D.-Y. Choi, "Study on mutual coupling reduction technique for MIMO antennas," *IEEE Access*, Vol. 2018, 2885558, 1–25, 2018.
14. Zhao, L. and K.-L. Wu, "A dual-band coupled resonator decoupling network for two coupled antennas," *IEEE Transactions on Antennas and Propagation*, Vol. 63, No. 7, 2843–2850, Jul. 2015.
15. Mashagba, H. A., H. A Rahim, I. Adam, et al., "A hybrid mutual coupling reduction techniquein a dual-band MIMO textile antenna for WBAN and 5G applications," *IEEE Access*, Vol. 9, No. 12, 150768–150780, Oct. 2021.
16. Guo, J.-Y., F. Liu, G.-D. Jing, L.-Y. Zhao, et al., "Mutual coupling reduction of multiple antenna systems," *Frontiers of Information Technology & Electronic Engineering*, Vol. 21, No. 3, 366–376, 2020.
17. Al-Hasan, M., I. B. Mabrouk, E. R. F. Almajali, M. Nedil, and T. A. Denidni, "Hybrid isolator for mutual-coupling reduction in MMW MIMO antenna systems," *IEEE Access*, Vol. 7, 58466–58474, 2019.
18. Lee, W.-W. and B. Jang, "2×2 MIMO antenna system with different antenna types for mobile terminals," *Microwave and Optical Technology Letters*, Vol. 58, No. 6, 1337–1340, Jun. 2016.
19. Iqbal, A., O. A. Saraereh, A. W. Ahmad, and S. Bashir, "Mutual coupling reduction using F-shaped stubs in UWB-MIMO antenna," *IEEE Access*, Vol. 6, 2755–2759, 2018.
20. Zhang, Q.-L., Y.-T. Jin, J.-Q. Feng, X. Lv, and L.-M. Si, "Mutual coupling reduction of microstrip antenna array using metamaterial absorber," *IEEE Xplore*, 1–3, 2015.
21. Alibakhshikenari, M., A. Salvucci, G. Polli, B. S. Virdee, et al., "Mutual coupling reduction using metamaterial supersubstrate for high performance & densely packed planar phased arrays," *IEEE Transactions on Antennas and Propagation*, Vol. 64, No. 5, 1653–1660, May 2016.
22. Saxena, G., P. Jain, and Y. K. Awasthi, "High diversity gain MIMO-antenna for UWB application with WLAN notch band characteristic including human interface devices," *Wireless Personal Communications*, Vol. 112, No. 1, 105–121, 2019.

23. Yadav, D., M. P. Abegaonkar, S. K. Koul, V. N. Tiwari, and D. Bhatnagar, "Two element band-notched UWB MIMO antenna with high and uniform isolation," *Progress In Electromagnetics Research M*, Vol. 63, 119–129, 2018.
24. Singh, H. S., *Investigations of MIMO Antenna for Smart Mobile Handsets and Their User Proximity*, 23–32, Intech Open, 2019.